




# Synthetic Aperture Radar Interference Based on Scene Fusion and Active Cancellation

Qizhen Zhou, *Graduate Student Member, IEEE*, Song Zhou , *Member, IEEE*, Lei Yang , *Member, IEEE*, Xiao Ning, *Graduate Student Member, IEEE*, and Mengdao Xing , *Fellow, IEEE*

**Abstract**—Echo cancellation is used for eliminating echo signals by signal modulation in the frequency domain and time domain. However, it depends on the high accuracy of parameter estimation. In addition, it introduces an incompatible black mark in the synthetic aperture radar (SAR) image, which will be easily detected and inevitably degrades the deception performance. To address this problem, this article proposed a compound interference method that combines echo cancellation and deception jamming. In order to fuse the deception scene with the surrounding scene, the optimal deception template is generated by using the scene around the target of interest (TOI), and the deception template is used to modulate the coefficient of the original signal to generate the deception signal. Then, the deception signal is sent to the SAR platform together with the cancellation signal, which is generated by an active source. After the SAR process, the incompatible black mark in the image is replaced by a template with high similarity of surrounding scene, which effectively improves the deception performance. The proposed method can be used to cover the higher scattering characteristic of the TOI with the lower scattering characteristic of the deception template. Simulation results are provided and analyzed to validate the universality and the performance superiority of the proposed method.

**Index Terms**—Coefficient modulation, deception template, echo cancellation, synthetic aperture radar (SAR).

## I. INTRODUCTION

**S**YNTHETIC aperture radar (SAR) is widely used in military and civil fields because of its high-resolution imaging capability in all day-and-night and all weather [1]–[6]. With the development of SAR technology, new requirements and challenges have been put forward to SAR jamming deception to protect the target of interest (TOI) [7] being detected by the SAR platform. In the past few decades, a large number of

new interferences have been developed [8]–[10], which greatly enriches the method of the SAR jamming theory and improves the jamming performance.

Most SAR jamming is to suppress the TOI by sending noise pollution signal [11], or sending multiple false target signal that is highly similar to TOI echo signal [12]. These jamming methods can protect TOI from being easily recognized by SAR. But there is a common problem: TOI still exists in the SAR image, which has the danger to expose the TOI location.

In order to eliminate the TOI from SAR image, echo cancellation is proposed in recent years [13]–[16]. The principle of echo cancellation is that the echo signal is received by the canceller, and then, the cancellation signal with equal amplitude and opposite phase is generated [17]. By using the method proposed in [18], the problem of time-domain synchronization with real signals caused by the delay is addressed. On this basis, interrupted-sampling repeater jamming (ISRJ) is proposed [19], [20], which provides a new coherent interference mode for combating bandwidth radar. ISRJ allows a single antenna jammer to periodically sample and repeat a portion of the intercepted signal, which can be processed to form multiple false targets [21]. However, the multiple false targets are still in the SAR image and they are easily detected.

To improve the deception performance, the modified SAR echo cancellation is proposed in [22], which can cancel the target echo by the jamming strip. But there will be a similar interference area covered by strong noise on the SAR image. Although the amplitude mismatch can be reduced to some extent, but this interference region is still easily detected because of its incompatible scattering characteristics.

How to protect TOI from being detected and recognized by the SAR sensor is still a challenge. This article proposed a compound jamming strategy based on scene fusion and active cancellation. In the active cancellation, the target echo is modulated by time delay and frequency shift to generate a signal with the same amplitude and opposite phase of the target echo so that the TOI can be eliminated in the image after SAR processing. Then, in the jamming process, we sample the scattering coefficient of the scene around the TOI and generate the deception template to cover the cancellation region. In order to make the template have high deception performance, the new method of calculating the optimal value is proposed. The optimal value is calculated by minimizing the difference of scene scattering characteristics after the fusion process so that the deception template has high compatibility performance.

Manuscript received June 12, 2021; revised August 22, 2021; accepted October 1, 2021. Date of publication October 6, 2021; date of current version October 25, 2021. This work was supported in part by the National Natural Science Foundation of China under Grants 61801204 and 62061031, and in part by the public foundation from Key Laboratory of EMW Information, Fudan University, China, under Grant EMW201901. (*Corresponding author: Song Zhou.*)

Qizhen Zhou, Song Zhou, and Xiao Ning are with the School of Information Engineering, Nanchang University, Nanchang 330031, China (e-mail: 1012574027@qq.com; zhousong8411@sina.com; 1959952592@qq.com).

Lei Yang is with the Tianjin Key Lab for Advanced Signal Processing, Civil Aviation University of China, Tianjin 300300, China (e-mail: yanglei840626@163.com).

Mengdao Xing is with the National Laboratory of Radar Signal Processing, Xidian University, Xi'an 710071, China, and also with the Collaborative Innovation Center of Information Sensing and Understanding, Xidian University, Xi'an 710071, China (e-mail: xmd@xidian.edu.cn).

Digital Object Identifier 10.1109/JSTARS.2021.3117849

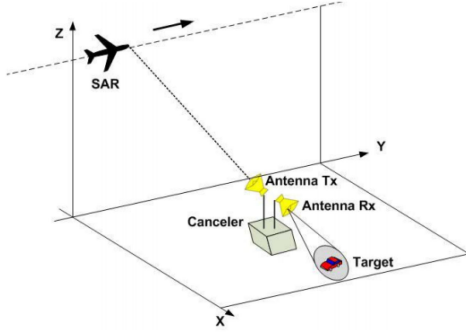


Fig. 1. Geometry of SAR, interference system, and target.

After the deception template is obtained, the original signal is modulated and transmitted back to the SAR along with the cancellation signal. In the end, there is only one deception scene in the TOI of the SAR image that is highly similar to the surrounding scene, which makes the TOI “disappear” from the SAR image. So, the jamming method has a high performance. Because the deception scenario is covered in the region after cancellation, it has a high tolerance of error with high robustness. In most interference methods, the scattering characteristic of the deception template is required to be higher than that of the covered scene. However, the proposed method can be used to cover the higher scattering characteristic of the TOI with the lower scattering characteristic of the deception template, which shows that the proposed method has universality and practicability.

The rest of this article is organized as follows. The second section introduces the signal model and the cancellation principle. The third section introduces the principle of jamming and the improved method. Section IV proves the effectiveness of this method by simulation and measured data. Finally, Section V concludes this article.

## II. SIGNAL MODEL AND CANCELLATION PRINCIPLE

Fig. 1 shows the geometric model of the SAR interference system, which protects the TOI from airborne SAR recognition. Antenna TX points to the SAR, while antenna RX points to the target. TX is for receiving origin signal and sending echo signal, and RX is for receiving echo signal. The aircraft flies along the dotted line in the direction of the arrow, and the interference system is located in the line of sight of the SAR sensor. SAR sensor, target, and interference system are set to be on the same line.

The interference signal generation steps are shown in Fig. 2. The original signal is transmitted from SAR sensor to Tx, and the jammer receives the original signal from Tx, then modulates its coefficient, and generates the jamming signal. At the same time, RX receives the echo signal, and the cancellation signal is generated by the canceller, which is transmitted back to the SAR sensor together with the jamming signal.

$S(t)$  denotes the transmit signal of the SAR sensor, and the center frequency of the signal is  $f_0$ . The chirp rate is  $k$ .  $S(t)$  can

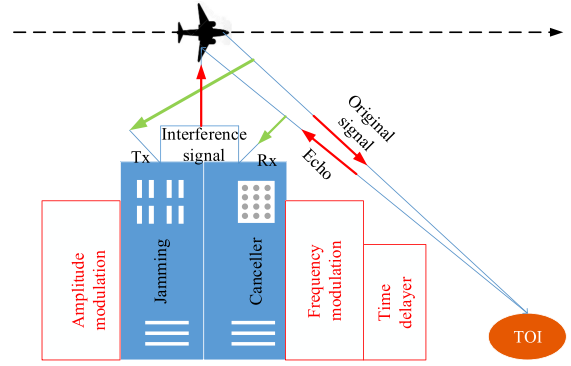


Fig. 2. Process of the interference.

be expressed as

$$S(t) = \text{rect}\left(\frac{t}{T}\right) \exp\left(j2\pi f_0 t + j\pi k t^2\right) \quad (1)$$

where  $t$  is the fast time variable, and  $T$  is the pulsewidth. After demodulation, the baseband echo can be written as

$$S_c(t_r, t_m) = \text{rect}\left[\frac{t_r - \frac{2R(t_m)}{c}}{T}\right] \exp\left[j2\pi f_0 \frac{2R(t_m)}{c}\right] \times \exp\left\{j\pi k \left[t_r - \frac{2R(t_m)}{c}\right]^2\right\} \quad (2)$$

where  $t_r$  denotes the fast time, and  $t_m$  denotes the slow time.  $R(t_m)$  is the distance between the target and radar and  $c$  is the speed of light. After a series of procedures, the final image can be obtained, given as

$$I_c(t_r, t_m) = \text{sinc}\left[\left(t_r - \frac{2R_{\min}}{c}\right)B_r\right] \text{sinc}\left[\left(t_m - t_{\min}\right)B_a\right] \times \exp\left(-j2\pi f_0 \frac{2R_{\min}}{c}\right) \quad (3)$$

where  $R_{\min}$  denotes the minimum distance between radar and target,  $t_{\min}$  is the slow time when SAR is closest to the target, and  $B_r$  is signal bandwidth.  $B_a$  is azimuth bandwidth,  $\text{sinc}(x) = \sin(\pi x)/\pi x$ .

In order to eliminate the real signal echo of interest, the cancellation signal should be satisfied

$$S_r(t_r, t_m) = -S_c(t_r, t_m). \quad (4)$$

However, (4) is just the ideal situation. Actually, the cancellation processing signal will inevitably introduce delay. The cancellation signal is

$$S_{rd}(t_r, t_m) = -S_c(t_r - t_d, t_m). \quad (5)$$

This causes the cancellation signal lag behind the real signal in time domain. By using the coupling property of the linear frequency modulation signal in the time domain and frequency domain, the frequency shift of  $f_d$  is added to the cancellation

signal. The cancellation signal can be given as

$$\begin{aligned}
 S_i(t_r, t_m) &= \text{rect} \left[ \frac{t_r - \frac{2R(t_m)}{c} - t_d}{T} \right] \exp \left[ j2\pi f_0 \frac{2R(t_m)}{c} \right] \\
 &\times \exp \left\{ j\pi k \left[ t_r - \frac{2R(t_m)}{c} - t_d \right]^2 \right\} \\
 &\times \exp(-j2\pi f_0 t_d) \exp \left\{ j\pi f_d \left[ t_r - \frac{2R(t_m)}{c} - t_d \right] \right\}. \quad (6)
 \end{aligned}$$

After imaging processing, the final result can be given as

$$\begin{aligned}
 I_i(t_r, t_m) &= \text{sinc} \left[ \left( t_r - \frac{2R_{\min}}{c} - t_d + \frac{f_d}{k} \right) B_r \right] \\
 &\times \text{sinc} \left[ \left( t_m - t_{\min} \right) B_a \right] \exp \left( -j2\pi f_0 \frac{2R_{\min}}{c} \right) \\
 &\times \exp \left[ -j\pi \left( \frac{f_d^2}{k} + 2f_0 t_d \right) \right] \\
 &= I_c \left( t_r - t_d + \frac{f_d}{k}, t_m \right) \exp \left[ -j\pi \left( \frac{f_d^2}{k} + 2f_0 t_d \right) \right]. \quad (7)
 \end{aligned}$$

When  $f_d$  and  $t_d$  in (7) satisfy

$$\begin{cases} f_d = -f_0 + \sqrt{f_0^2 + (2i+1)k} \\ t_d = \frac{f_d}{k} \end{cases} \quad (8)$$

where  $i$  is an integer. According to (8), the cancellation signal has the opposite phase to the real echo signal. In order to equalize the amplitude of the cancellation signal and the real echo signal, the transmitting power of the canceller must be satisfied [18]

$$P_{tx}(t_m) = P_{rx}(t_m) \frac{(4\pi R_c)^2}{\lambda^2 G_{tx} G_{rx}} \quad (9)$$

where  $P_{rx}(t_m)$  represents the magnitude of the echo from the target received by Rx, and  $\lambda$  is the signal wavelength.  $G_{tx}$  is the gain of the transmitting antenna of the canceller, while  $G_{rx}$  is the gain of the receiving antenna.  $R_c$  is the distance from the target to the canceller. Then, a cancellation signal is obtained with equal in amplitude and opposite in phase to the target echo so that the sum of  $I_i(t_r, t_m)$  and  $I_c(t_r, t_m)$  becomes zero and TOI will disappear from the SAR image.

In this section, we described the process of canceling the signal generation. In the following section, we will discuss how to generate the jamming signal.

### III. THEORY OF JAMMING

In the second section, the generation of the cancelling signal is described. In this section, we will discuss how to generate the jamming signal. First, the generation of the jamming signal is to extract the scattering characteristics around the protected target, then save it to the database. Second, after Tx receives the original signal, the signal coefficient is modulated by the jammer. Then, the jamming signal with the scattering characteristic of the surrounding scene is generated, and transmitted back to the SAR sensor with the cancellation signal. Finally, in the final imaging

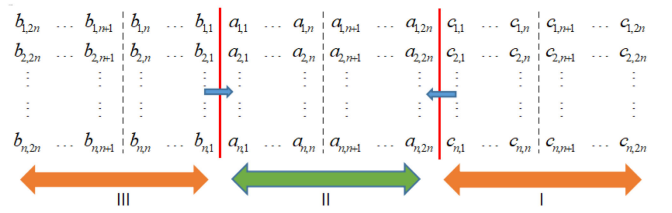


Fig. 3. Distribution of scattering coefficients of targets and surrounding scenes.

results, only the deception scene integrates with the surrounding scene appears at the TOI. In order to make the jamming scene more compatible with the surrounding scene, a new strategy is proposed and discussed in the following.

First, the scattering coefficient around TOI is extracted. Fig. 3 shows the distribution of scattering coefficients of the target and the surrounding scenes. To facilitate the analysis, the shape of the protection target is set to be a rectangle. Areas I and III represent the surrounding scene, and area II represents the protected target.  $A$  is the coefficient matrix of the target to be protected,  $B$  and  $C$  are the coefficient matrices of the surrounding scene stored in the database.  $A$ ,  $B$ , and  $C$  can be written as

$$A = \begin{Bmatrix} a_{1,1} & \dots & a_{1,2n} \\ \vdots & \dots & \vdots \\ a_{n,1} & \dots & a_{n,2n} \end{Bmatrix} \quad (10)$$

$$B = \begin{Bmatrix} b_{1,1} & \dots & b_{1,2n} \\ \vdots & \dots & \vdots \\ b_{n,1} & \dots & b_{n,2n} \end{Bmatrix} \quad (11)$$

and

$$C = \begin{Bmatrix} c_{1,1} & \dots & c_{1,2n} \\ \vdots & \dots & \vdots \\ c_{n,1} & \dots & c_{n,2n} \end{Bmatrix}. \quad (12)$$

In general, there are differences in scattering coefficients under different scenes. For a more intuitive analysis, the difference can be denoted by  $D(i, j)$  and given as

$$\begin{cases} D_b(i, j) = \sqrt{\sum_{q=1}^n (a_{q,i} - b_{q,j})^2} \\ D_c(i, j) = \sqrt{\sum_{q=1}^n (a_{q,i} - c_{q,j})^2} \end{cases} \quad (13)$$

where  $i$  and  $j$  represent the columns in matrices  $A$  and  $B$  or  $C$ , respectively. Let  $a_{q,i}$  the  $i$ th column element in  $A$ , be the mean value of each row. Then,  $D_b(i, j)$  is the variance of the  $j$ th column element in the matrix  $B$ , and  $D_c(i, j)$  is the variance of the  $j$ th column element in the matrix  $C$ . As shown in Fig. 4, if area III is used as the deception scenario, it has

$$A = \begin{Bmatrix} b_{1,2n} & \dots & b_{1,1} \\ \vdots & \dots & \vdots \\ b_{n,2n} & \dots & b_{n,1} \end{Bmatrix}. \quad (14)$$

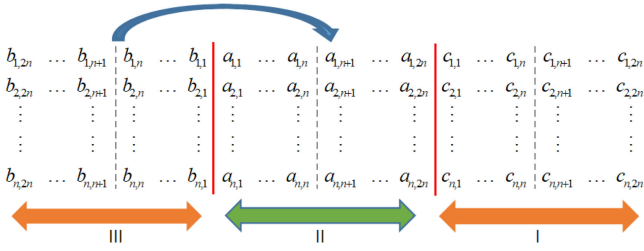


Fig. 4. B as the deception scenario.

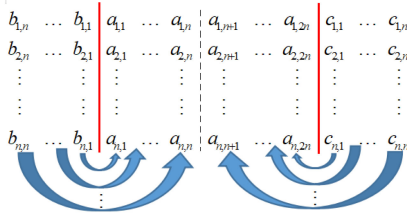


Fig. 5. Sampling in reverse sort.

Then,  $D_b(1, 1)$  and  $D_c(2n, 1)$  are given by

$$D_b(1, 1) = \sqrt{\sum_{q=1}^n (a_{q,1} - b_{q,1})^2} = \sqrt{\sum_{q=1}^n (b_{q,2n} - b_{q,1})^2} \quad (15)$$

and

$$D_c(2n, 1) = \sqrt{\sum_{q=1}^n (a_{q,2n} - c_{q,1})^2} = \sqrt{\sum_{q=1}^n (b_{q,1} - c_{q,1})^2}. \quad (16)$$

In the scene with more uniform scattering characteristics,  $D_b(1, 1)$  and  $D_c(2n, 1)$  are relatively small, this indicates that the deception scene blends well with the surrounding scene. However, the scene is not evenly distributed in practical application, and the values of  $D_b(1, 1)$  and  $D_c(2n, 1)$  vary greatly. It makes the deception scenario even more incompatible with the surrounding scene, and makes the TOI easy to be detected and recognized by the SAR sensor.

In order to reduce the value of  $D(i, j)$ , we can use the reverse sort to eliminate the difference at the scene boundary. Reverse sort is to replace the first  $n$  column elements of the matrix  $A$  by the first  $n$  column elements of the matrix  $B$ , and to replace the last  $n$  column elements of the matrix  $A$  by the first  $n$  column elements of the matrix  $C$ . As shown in Fig. 5, matrix  $A$  becomes

$$A = \begin{Bmatrix} b_{1,1} & \dots & b_{1,n} & c_{1,n} & \dots & c_{1,1} \\ \vdots & \vdots & \vdots & \vdots & \vdots & \vdots \\ b_{n,1} & \dots & b_{n,n} & c_{n,n} & \dots & c_{n,1} \end{Bmatrix}. \quad (17)$$

And it has

$$D_b(1, 1) = \sqrt{\sum_{q=1}^n (a_{q,1} - b_{q,1})^2} = \sqrt{\sum_{q=1}^n (b_{q,1} - b_{q,1})^2} = 0 \quad (18)$$

and

$$D_c(2n, 1) = \sqrt{\sum_{q=1}^n (a_{q,2n} - c_{q,1})^2} = \sqrt{\sum_{q=1}^n (c_{q,1} - c_{q,1})^2} = 0. \quad (19)$$

Equations (18) and (19) show that the deception scene is well integrated with the surrounding scene on the boundary, and there is no prominent part so that the deception performance is improved. Then, we get the corresponding value of  $D_c(n, n) = \sqrt{\sum_{q=1}^n (b_{q,n} - c_{q,n})^2}$ , which is in the middle of this deception template.

However, as the scattering characteristics of the area III is quite different from area I, the value of  $D_c(n, n)$  becomes larger. This leads to more incompatibility in the center of the scene. To address this problem, an improved method is proposed. Based on the reverse sampling, the scene boundary is fused without difference. The optimal value is calculated to minimize the value of  $D(i, j)$ .

Let  $P_k$  be the differences between the elements in the columns of the coefficient matrices  $B$  and  $C$ , given as

$$P_k(i) = |b_{i,k} - c_{i,2n-k}| \quad k = 1, 2, \dots, 2n \quad (20)$$

where  $P_k(i)$  is the difference between the coefficient matrices of  $A$  and  $B$  in each column of the  $i$ th row. After sampling the scattering coefficients of area III and area I, we can obtain the coefficient matrices of  $B$  and  $C$ . Without the loss of generality, it is assumed that  $B$  and  $C$  are different from each other. The larger the value of  $P_k(i)$  is, the greater the difference between the elements in a column of  $B$  and  $C$  becomes. Conversely, the smaller the  $P_k(i)$  value is, the smaller the difference becomes. Calculating the optimal value is to find the value of  $k$  that minimizes the value of  $P_k(i)$ . By Arranging the values of  $P_k(i)$  to calculate the minimum value, we can use  $m$  to represent  $k$  values that minimize  $P_k(i)$  values. It satisfies

$$P_m(i) \leq P_k(i) \quad m, k = 1, 2, \dots, 2n \quad (21)$$

where  $P_m(i)$  is the optimal value calculated in each row.  $m$  can be regarded as a position where the difference between the  $m$  column of  $B$  and the  $2n - m$  column of  $C$  is minimal in each row. Then,  $P_m$  is given by

$$P_m = \{P_m(1), P_m(2), \dots, P_m(n)\}. \quad (22)$$

It means that in each row, the first  $m$  columns in the matrix  $B$  and the first  $2n - m$  columns in the matrix  $C$  form the matrix  $A$ . We can get the coefficient matrix of  $A$ , given as

$$A = \begin{Bmatrix} b_{1,1} & \dots & b_{1,m} & c_{1,2n-m} & \dots & c_{1,1} \\ \vdots & \vdots & \vdots & \vdots & \vdots & \vdots \\ b_{n,1} & \dots & \dots & b_{n,m} & c_{n,2n-m} & \dots & c_{n,1} \end{Bmatrix}. \quad (23)$$

At the left and right solid boundaries of the deception scenario,  $D_b(1, 1)$  and  $D_c(2n, 1)$  are equal to 0. At the junction of each row,  $P_m$  is the optimal value. The whole deception scene can be well compatible with the surrounding scene, and it has high deception performance. Then, the signal collected by Tx is modulated by the deception template to generate the jamming signal.



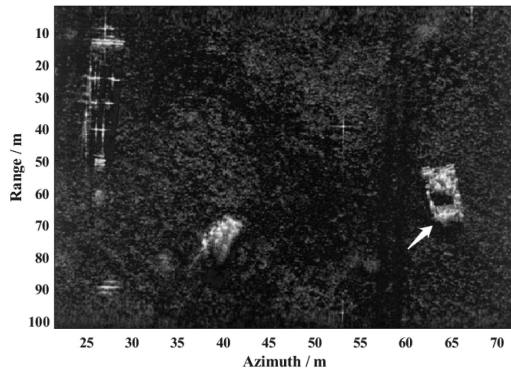


Fig. 6. Origin image.

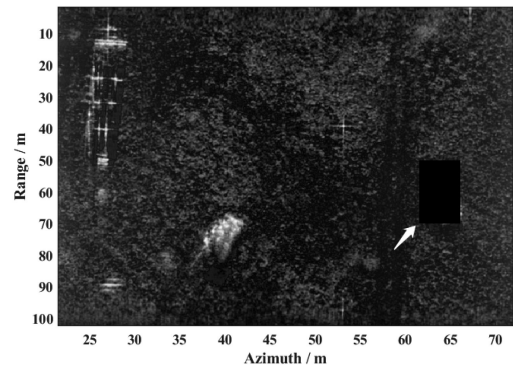


Fig. 7. Cancellation result.

If the pulse compressed signal does not carry the scattering information of the object, the baseband echo signal is according to (2). After coefficient modulation, the result becomes

$$\begin{aligned}
 S_d(t_r, t_m) &= \sum_{x=1}^n \sum_{y=1}^{2n} a_{(x,y)} \text{rect} \left( \frac{t_r - \frac{2R(t_m)}{c}}{T} \right) \\
 &\times \exp \left\{ j2\pi f_0 \frac{2R(t_m)}{c} \right\} \\
 &\times \exp \left\{ j\pi k \left[ t_r - \frac{2R(t_m)}{c} \right]^2 \right\}. \quad (24)
 \end{aligned}$$

The final compound interference signal is

$$S_f(t_r, t_m) = S_d(t_r, t_m) + S_i(t_r, t_m). \quad (25)$$

So far, the interference signal is obtained. The deception template will replace the TOI in the SAR image with a high deception performance.

#### IV. SIMULATION AND ANALYSIS

In this section, a SAR image from the US Sandia National Laboratories is used for simulation, which is obtained from the SAR platform working in Ku band [23]. The SAR operates at 12 GHz, and the chirp rate is  $1.5 \times 10^{14}$  Hz/s. By echo simulation, the imaging experiment is carried out by using the range Doppler algorithm. The SAR platform flies at 50 m/s, with a range resolution of 0.25 m and an azimuth resolution of 0.59 m.

Fig. 6 is the original image, the white arrow is added by the author, and the arrow indicates the target to be protected. By using the method mentioned in [18] to actively cancel the echo of target, the results are shown in Fig. 7. It can be seen from Fig. 7 that the target indicated by the white arrow has been replaced by a black mark. It can be easily detected by the SAR sensor.

To improve deception performance, the method proposed in Fig. 4 is implemented. The region on the right side of the target is used for the deception scenario. Under the combined action of the jamming signal and the cancellation signal, the black mark in Fig. 7 will be covered by the right deception scene, and the result is shown in Fig. 8. In Fig. 8, significant gaps can be seen at the boundary of the covered area, as shown by the white arrows. The left arrow represents  $D_b(1,1)$ , and the

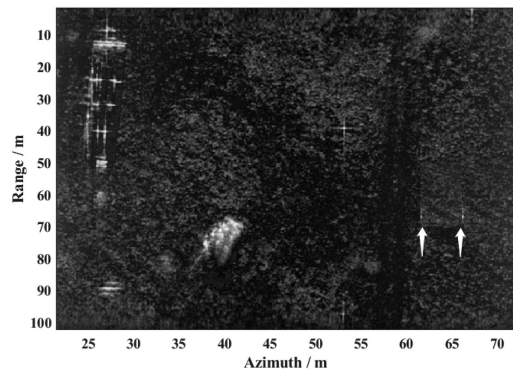


Fig. 8. Results of the first deception scheme.

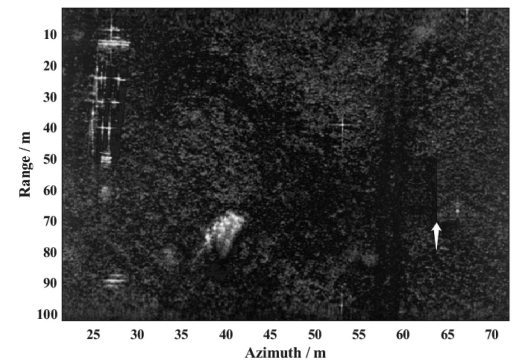


Fig. 9. Results of improved methods.

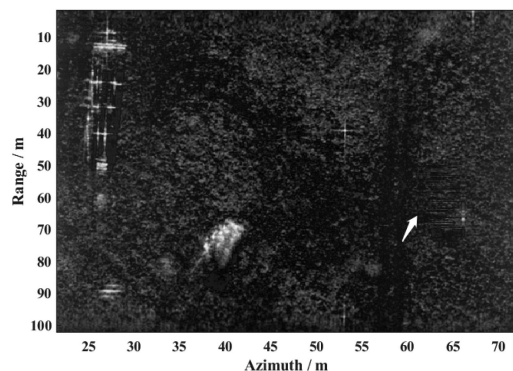


Fig. 10. Imaging results of the final proposed method.

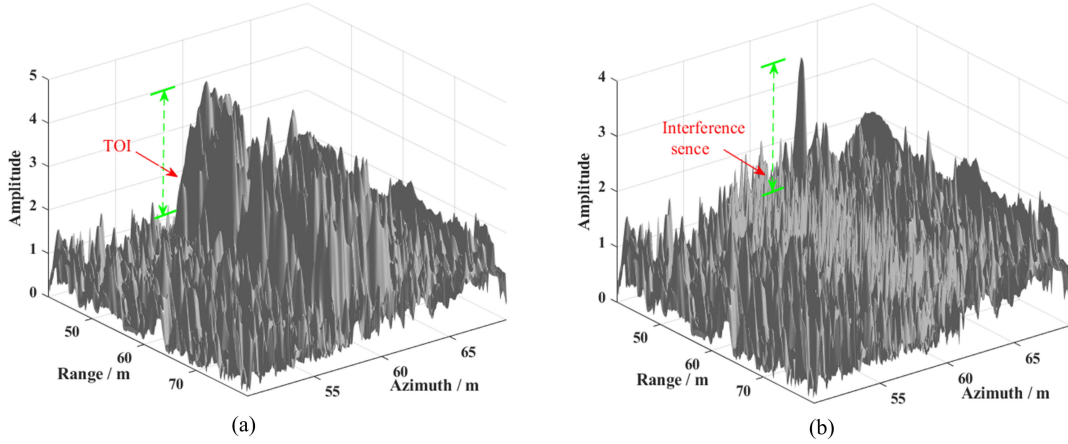


Fig. 11. Simulation results of 3-D. (a) Origin position of the target. (b) Result after interference.

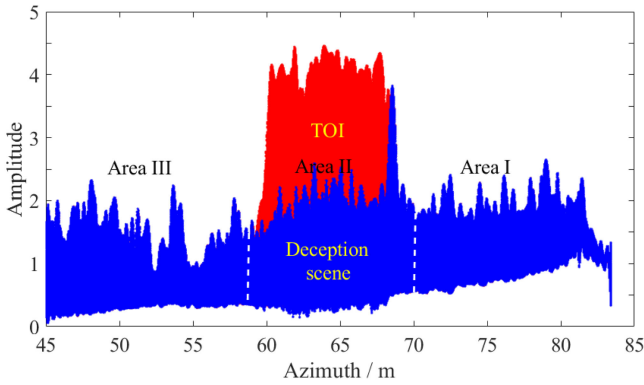


Fig. 12. Comparison of amplitude in different area.

right arrow represents  $D_c(2n, 1)$ . It can be seen from Fig. 8 that the deception performance is degraded seriously because of the large values of  $D_b(1, 1)$  and  $D_c(2n, 1)$ . Then, we implement the other method proposed in Fig. 5, and the results are shown in Fig. 9. It can be seen that the two gaps in Fig. 8 have disappeared, and the boundary is better compatible with the surrounding environment, and the deception performance is improved. However, the significant gap is still in the middle of the deception scene in the image, which is consistent with the larger value of the  $D_c(n, n)$  aforementioned. When the scattering coefficients of the scene around the TOI are evenly distributed, the methods described in Figs. 4 and 5 can be applied in practice. But most of the time, they are quite different, and the incompatibility will also introduce the danger of SAR detection.

Then, we utilize the method described in Fig. 5 by minimizing the value of  $P_k$ . The simulation results are shown in Fig. 10. Comparing with Fig. 9, the gap in the middle of the image has disappeared. In Fig. 10, the deception scene is well compatible with the surrounding scene. Fig. 11 evaluates the interference performance by observing the amplitude of the scene. In Figs. 11 and 12, we make the quantitative evaluation of the deception scene. The amplitude of the TOI is significantly higher than that of the surrounding scene, and after the interference, the target

has been replaced by the deception scene. The effectiveness and superiority of the proposed method are verified. It is also important to note that when the scattering characteristic of the TOI is quite different from the surrounding scene, a deception result with high performance can still be obtained. It indicates the universality of the proposed method.

Now, we discuss the robustness of the proposed method. The performance of the proposed method is highly dependent on parameters. When the power of the canceller is lower than the standard value, the residual of the cancellation signal is still in the image. The deception performance will be degraded when the power of the jammer is low. By using the error to represent the amplitude mismatch,  $e_1$  indicates the cancellation error, and  $e_2$  indicates the deception error. The errors are given by

$$e_1 = \frac{|X_{j\text{real}} - Y|}{Y}$$

$$e_2 = \frac{|X_{c\text{real}} - Y|}{Y} \quad (26)$$

where  $X_{j\text{real}}$  denotes the amplitude of the signal sent by the jammer and  $X_{c\text{real}}$  denotes the amplitude of the signal sent by the canceller, and  $Y$  denotes the amplitude of the target.

As shown in Fig. 13, when  $e_1$  is assumed to be 0.2, the outline of the target can be seen, but it is not clear. When  $e_1$  increases to 0.4, it can be clearly seen that the target still exists in the SAR image. The cancellation performance degrades seriously. When the deception scene is added, the result is shown in Fig. 14. By comparing Fig. 14(a) with Fig. 13(a), there is no outline of the TOI in Fig. 14(a). The deception scene is compatible with the surrounding scene, and the TOI is well hidden. When  $e_1$  increases to 0.4, the TOI is still difficult to be detected by the SAR sensor as shown in Fig. 14(b). When  $e_1$  increases to 0.6, the performance of the proposed method is degraded obviously since the TOI has a strong scattering characteristic and the deception scene has a weak scattering characteristic. However, the deception performance in Fig. 14(c) is still higher than in Fig. 13(b). It indicates that the proposed method has higher robustness. When  $e_2$  is not equal to 0, the interference result is shown in Fig. 15. By comparing Fig. 15 with Fig. 14(a),



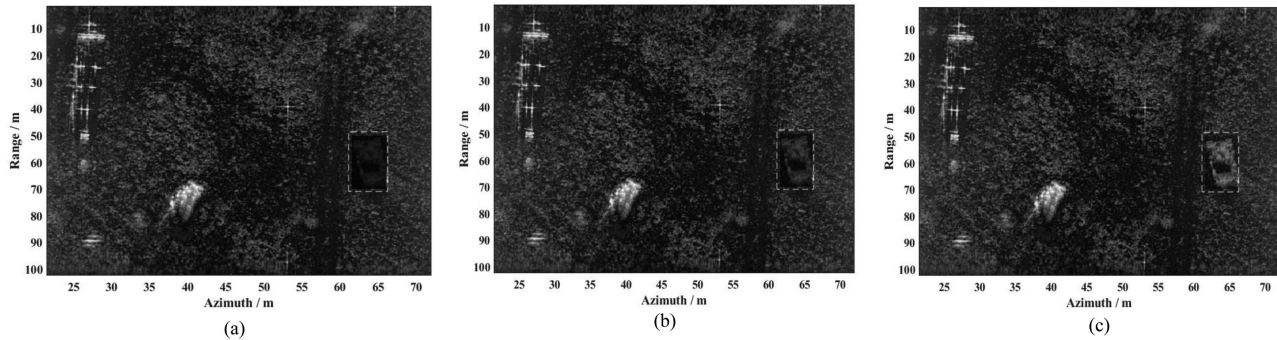


Fig. 13. Simulation results after cancellation. (a) Cancellation result for  $e_1 = 0.2$ . (b) Cancellation result for  $e_1 = 0.4$ . (c) Cancellation result for  $e_1 = 0.6$ .

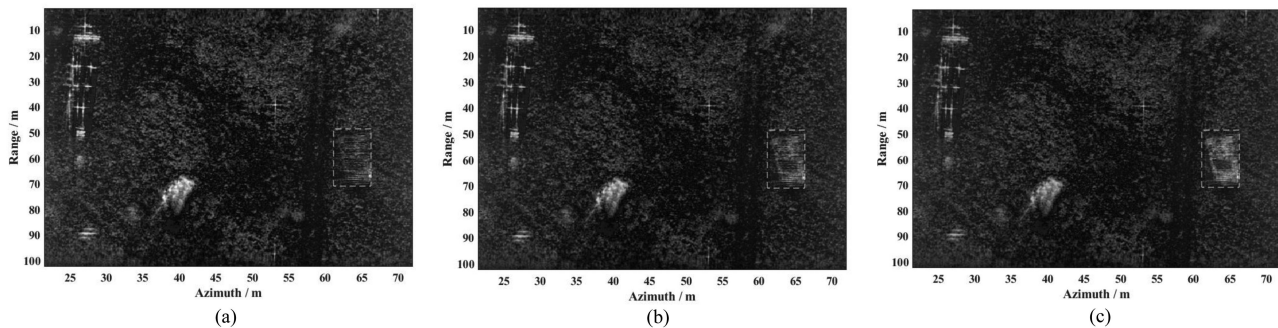


Fig. 14. Simulation results after interference. (a) Interference result for  $e_1 = 0.2$  and  $e_2 = 0$ . (b) Interference result for  $e_1 = 0.4$  and  $e_2 = 0$ . (c) Interference result for  $e_1 = 0.6$  and  $e_2 = 0$ .

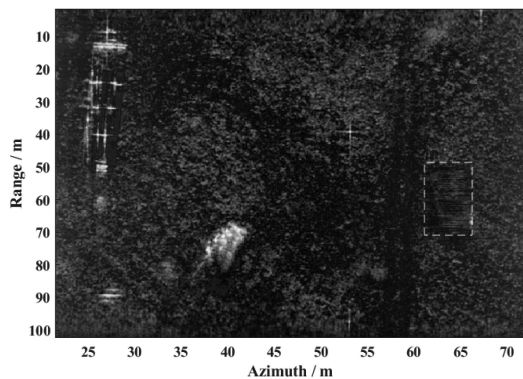


Fig. 15. Simulation results for  $e_1=0.2$  and  $e_2=0.4$ .

they both achieve high performance. This indicates that the interference performance is insensitive to the jammer error when the scattering characteristic of the target is significantly higher than the deception scene.

So far, the effectiveness and high performance of the proposed method are verified in Fig. 10, and the deception scene is well compatible with the surrounding scene. It can also be found that the final deception performance is related to the deception scene, and the scattering characteristics of the real scene as well as the errors of the canceller and jammer. When the scattering coefficient of the real scene is much higher than that of the deception scene, the interference performance will highly depend on the error of the canceller. When the scattering coefficient of

the deception scene is higher, the interference performance will highly depend on the error of the jammer.

## V. CONCLUSION

This article proposed a compound interference method that combines echo cancellation and deception jamming. After eliminating the real target in the SAR image, the interference system produces deception scene that fuses with the surrounding scene, and it is not easy to be detected by the SAR sensor. By comparing with the original method, the proposed method has higher robustness and interference performance. In practice, the proposed method can protect some important military targets from the SAR detection. Finally, we analyze the factors that affect the interference effect, which will facilitate the design of the actual interference system. When the scattering coefficient of the protected target is higher than the surrounding scene, the error of the canceller should be reduced as much as possible, which can improve the interference performance.

## REFERENCES

- [1] M. Zink *et al.*, "Tandem-x: 10 years of formation flying bistatic SAR interferometry," *IEEE J. Sel. Topics Appl. Earth Observ. Remote Sens.*, vol. 14, pp. 3546–3565, 2021.
- [2] A. Moreira, P. Prats-Iraola, M. Younis, G. Krieger, I. Hajnsek, and K. P. Papathanassiou, "A tutorial on synthetic aperture radar," *IEEE Geosci. Remote Sens. Mag.*, vol. 1, no. 1, pp. 6–43, Mar. 2013.
- [3] W. Pu, "Shuffle GAN with autoencoder: A deep learning approach to separate moving and stationary targets in SAR imagery," *IEEE Trans. Neural Netw. Learn. Syst.*, to be published, doi: [10.1109/TNNLS.2021.3060747](https://doi.org/10.1109/TNNLS.2021.3060747).

- [4] R. S. Harness and M. C. Budge, "A study on SAR noise jamming and false target insertion," in *Proc. IEEE SoutheastCon*, 2014, pp. 1–8.
- [5] S. Zhou, L. Yang, L. Zhao, and G. Bi, "Quasi-polar-based FFBP algorithm for miniature UAV SAR imaging without navigational data," *IEEE Trans. Geosci. Remote Sens.*, vol. 55, no. 12, pp. 7053–7065, Dec. 2017.
- [6] L. Yang, P. Li, S. Zhang, L. Zhao, S. Zhou, and M. Xing, "Cooperative multitask learning for sparsity-driven SAR imagery and nonsystematic error autocalibration," *IEEE Trans. Geosci. Remote Sens.*, vol. 58, no. 7, pp. 5132–5147, Jul. 2020.
- [7] J. Liu, M. Xing, H. Yu, and G. Sun, "EFTL: Complex convolutional networks with electromagnetic feature transfer learning for SAR target recognition," *IEEE Trans. Geosci. Remote Sens.*, to be published, doi: [10.1109/TGRS.2021.3083261](https://doi.org/10.1109/TGRS.2021.3083261).
- [8] F. Zhou, B. Zhao, M. Tao, X. Bai, B. Chen, and G. Sun, "A large scene deceptive jamming method for space-borne SAR," *IEEE Trans. Geosci. Remote Sens.*, vol. 51, no. 8, pp. 4486–4495, Aug. 2013.
- [9] H. Hu, X. Jia, Y. Wu, and J. Wu, "Research on the theory of 2-D interrupted sampling repeater scatter-wave jamming to SAR," *J. Acad. Equip. Command Technol.*, vol. 23, pp. 94–97, 2012.
- [10] Y. Liu, T. Li, and Z. Gu, "Research on SAR active deception jamming scenario generation technique," in *Proc. IEEE 5th Int. Conf. Instrum. Meas., Comput., Commun. Control*, 2015, pp. 152–156.
- [11] W. Ye, H. Ruan, S.-X. Zhang, and L. Yan, "Study of noise jamming based on convolution modulation to SAR," in *Proc. IEEE Int. Conf. Comput., Mechatronics, Control Electron. Eng.*, 2010, vol. 6, pp. 169–172.
- [12] Z. Bo, F. Zhou, X. Shi, Q. Wu, and B. Zheng, "Multiple targets deception jamming against iSAR using electromagnetic properties," *IEEE Sensors J.*, vol. 15, no. 4, pp. 2031–2038, Apr. 2015.
- [13] Y. Lu, R. Fowler, W. Tian, and L. Thompson, "Enhancing echo cancellation via estimation of delay," *IEEE Trans. Signal Process.*, vol. 53, no. 11, pp. 4159–4168, Nov. 2005.
- [14] X. Yang, W. Zhao, and L. Huang, "Calculation of RCS of targets and statistical analysis of cancellation effect," *Chin. J. Radio Sci.*, vol. 17, no. 1, pp. 88–92, 2002.
- [15] Y.-C. Xiang, C.-W. Qu, F. Su, and M.-J. Yang, "Active cancellation stealth analysis of warship for LFM radar," in *Proc. IEEE 10th Int. Conf. Signal Process.*, 2010, pp. 2109–2112.
- [16] Y. C. Xiang, C. B. QuLi, and H. Hou, "Simulation research on cancellation stealth of warship based on its radar scattering properties," *J. Syst. Simul.*, vol. 25, no. 1, pp. 104–110, 2013.
- [17] X. Sheng and X. Yuanming, "Simulation analysis of an active cancellation stealth system," *Optik*, vol. 125, no. 18, pp. 5273–5277, 2014.
- [18] L. Xu, D. Feng, Y. Liu, X. Pan, and X. Wang, "A three-stage active cancellation method against synthetic aperture radar," *IEEE Sensors J.*, vol. 15, no. 11, pp. 6173–6178, Nov. 2015.
- [19] X. S. Wang, J. C. Liu, W. M. Zhang, Q. X. Fu, Z. Liu, and X. X. Xie, "Mathematic principles of interrupted-sampling repeater jamming (isrj)," *Sci. China Ser. F, Inf. Sci.*, vol. 50, no. 1, pp. 113–123, 2007.
- [20] D. J. Feng, H. M. Tao, Y. Yang, and Z. Liu, "Jamming de-chirping radar using interrupted-sampling repeater," *Sci. China Inf. Sci.*, vol. 54, no. 10, pp. 2138–2146, 2011.
- [21] D. Feng, L. Xu, X. Pan, and X. Wang, "Jamming wideband radar using interrupted-sampling repeater," *IEEE Trans. Aerosp. Electron. Syst.*, vol. 53, no. 3, pp. 1341–1354, Jun. 2017.
- [22] Q. Wu, J. Liu, J. Wang, F. Zhao, and S. Xiao, "Improved active echo cancellation against synthetic aperture radar based on nonperiodic interrupted sampling modulation," *IEEE Sensors J.*, vol. 18, no. 11, pp. 4453–4461, Jun. 2018.
- [23] *The Sandia Complex Image Data*, 2006. [Online]. Available: <https://www.sandia.gov/radar/imagery/index.html>



**Qizhen Zhou** (Graduate Student Member, IEEE) was born in Jiangxi, Shangrao, China, in 1998. He received the B.S. degree in electronic information engineering from Gannan Normal University, Ganzhou, China, in 2019. He is currently working toward the M.S. degree in electronic communication engineering with Nanchang University, Nanchang, China.

His research interests include deception jamming of synthetic aperture radar (SAR) and forward-looking SAR.



**Song Zhou** (Member, IEEE) received the B.S. and M. S. degrees in telecommunication engineering and the Ph.D. degree in signal and information processing from Xidian University, Xi'an, China, in 2006, 2009, and 2013, respectively.

From January 2015 to February 2018, he was with the School of Electrical and Electronic Engineering, Nanyang Technological University, Singapore, as a Full-Time Research Fellow. He is currently working with the School of Information Engineering, Nanchang University, Nanchang, China. His research interests include monostatic/bistatic synthetic aperture radar applications and motion error compensation.



**Lei Yang** (Member, IEEE) was born in Tianjin, China, in 1984. He received the B.S. degree in electronic engineering and the Ph.D. degree in signal and information processing from Xidian University, Xi'an, China, in 2007 and 2012, respectively.

From December 2012 to February 2017, he worked with the School of Electrical and Electronic Engineering, Nanyang Technological University (NTU), as a Full Time Research Fellow and Temasek Lab, NTU, as a Research Scientist. He is currently working with the Tianjin Key Lab for Advanced Signal Processing, Civil Aviation University of China, as an Associate Professor. His main research interests include high-resolution radar imaging and implementation, sparse Bayesian learning for radar imaging, and so on.



**Xiao Ning** (Graduate Student Member, IEEE) was born in Hubei, China, in 1997. He received the B.S. degree from the Hubei University of Automotive Technology, Shiyan, China, in 2019. He is currently working toward the M.S. degree in electronic communication engineering with Nanchang University, Nanchang, China.

His research interests include passive synthetic aperture radar (SAR) and forward-looking SAR.



**Mengdao Xing** (Fellow, IEEE) received the B.S. and Ph.D. degrees from Xidian University, Xi'an, China, in 1997 and 2002, respectively.

He is currently a Professor with the National Laboratory of Radar Signal Processing, Xidian University, where he is also the Dean with the Academy of Advanced Interdisciplinary Research Department. His current research interests include synthetic aperture radar (SAR), SAR interferometry, inversed SAR, sparse signal processing, and microwave remote sensing. He has authored and coauthored more than 200

refereed scientific journal papers and two books about SAR signal processing. The total citation times of his research are greater than 10000 (H-index 50). He has achieved more than 50 authorized China patents.

Dr. Xing was rated as the Most Cited Chinese Researchers by Elsevier. His research has been supported by various funding programs, such as, National Science Fund for Distinguished Young Scholars. He has held several Special Issues on *IEEE Geoscience and Remote Sensing Magazine* and *IEEE Journal of Selected Topics in Applied Earth Observations and Remote Sensing*. He is currently an Associate Editor for radar remote sensing of the IEEE TRANSACTIONS ON GEOSCIENCE AND REMOTE SENSING and the Editor-in-Chief for *MDPI Sensors*.